J. Plasma Physics (2010), *vol.* 76, *parts* 3&4, *pp.* 513–523. © Cambridge University Press 2010
doi:10.1017/S0022377809990717

New aspects on plasma wave and instability phenomena in basic-plasma experiments

R. HATAKEYAMA[1], T. KANEKO[1] and W. OOHARA[2]

[1] Department of Electronic Engineering, Tohoku University, Sendai 980-8579, Japan (hatake@ecei.tohoku.ac.jp)

[2] Department of Electrical and Electronic Engineering, Yamaguchi University, Ube 755-8611, Japan

(Received 3 December 2009 and accepted 9 December 2009, first published online 15 January 2010)

Abstract. Our basic-plasma experiments relating to fusion-oriented and space plasmas have yielded deep and unique insight into wave and instability physics in ordinary electron-ion and unusual pair-particle plasmas. Here recent results on flow shears, polarization reversal and pair-ions are presented in the way that light is shed on the underlying physics.

1. Introduction

Plasma flows and their velocity shears in magnetized plasmas have attracted much attention not only in fusion-oriented plasmas but also in space plasmas, because the ion flow velocity shear parallel to magnetic field lines has been reported to enhance the ion-acoustic [1], ion-cyclotron [2] and drift-wave [3, 4] instabilities, while the perpendicular flow velocity shear has been confirmed to regulate not only the drift-wave but also ion-cyclotron instabilities independent of the sign of the shear [5]. In order to clarify the mechanisms of excitation and suppression of these instabilities in the real situation of the fusion and space plasmas, it is necessary to realize the controlled superposition of the parallel and perpendicular flow shears in basic-plasma experiments.

On the other hand, propagation and resonance absorption of an electron cyclotron wave are considered to be effective against plasma heating, formation of local confining potential in the fusion-oriented plasmas and homogeneous process-plasma productions. In these studies, the unexpected damping of a left-hand polarized wave (LHPW) near the electron cyclotron resonance (ECR) point was observed [6] and a polarization reversal was theoretically suggested in order to interpret the phenomenon. However, this polarization reversal has not been experimentally observed so far. In this sense, we have claimed that the detailed basic-plasma experiments are necessary to understand the absorption characteristics of the LHPW near the ECR point.

Furthermore, the plasma wave and instability phenomena not only in the above-mentioned typical plasmas consisting of electrons and positive ions but also in pair plasmas consisting of only positive- and negative-charged particles of equal mass have attracted special attention. Such pair plasmas maintain space-time symmetry because the mobility of the particles in electromagnetic fields is same. Some theoretical works have already been presented, which concern the elementary

https://doi.org/10.1017/S0022377809990717 Published online by Cambridge University Press

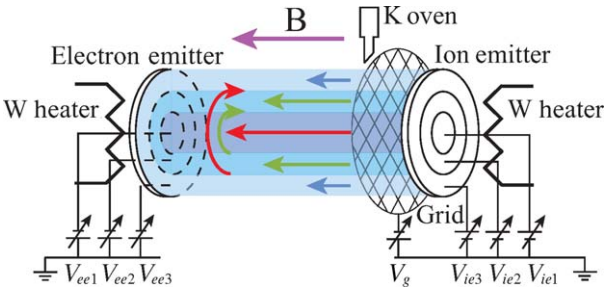


Figure 1. (Color online) Experimental setup for flow shear experiments.

properties and linear and nonlinear collective modes in non-relativistic electron-positron plasmas [7–9]. Plasmas including positrons have been generated experimentally in laboratories [10–12] but it is not easy to generate and maintain the electron-positron plasma for long duration. Therefore, our attention is concentrated on the easy and stable-state generation of a pair-ion plasma consisting of positive and negative ions of equal mass and its collective-mode identification.

Based on these backgrounds, the aim of the present work is to carry out the basic-plasma experiments on the ion flow shear modified drift-wave instabilities, polarization reversal of electromagnetic waves in magnetized plasmas and pair-ion plasmas in order to clarify the unsettled issues described above.

2. Low-frequency instabilities modified by flow shears

Low-frequency electrostatic instabilities modified by sheared plasma flows in magnetized plasmas are one of the very important issues in the field of the basic-plasma physics. In order to clarify the mechanisms of excitation and suppression of these instabilities, we externally and independently control the parallel and perpendicular flow shears in a basic-plasma device using three-segmented electron and ion sources.

2.1. Experimental setup

Experiments are performed in the Q_T-Upgrade machine of Tohoku University as shown in Fig. 1. We attempt to modify a plasma-synthesis method with opposed electron and potassium (K) ion emitters, where both the emitters are concentrically segmented into three sections [13]. When each section of the electron emitter is individually biased ($V_{ee1}, V_{ee2}, V_{ee3}$), the radially different plasma potential, *i.e.* radial electric field is generated. This electric field causes $E \times B$ flows and flow shears perpendicular to the magnetic field lines. On the other hand, the parallel ion flow with radially different energy, *i.e.* the parallel ion flow shear, is generated when each section of the segmented ion emitter is individually biased ($V_{ie1}, V_{ie2}, V_{ie3}$) at a positive value above the plasma potential that is determined by the bias voltage of the electron emitter. Therefore, these parallel and perpendicular flow shears can be superimposed by controlling the bias voltages of the ion and electron emitters independently. Under our conditions, the plasma density is 10^9 cm^{-1}, the electron temperature is 0.2 eV and the ion temperature is almost the same as the electron temperature. A background gas pressure is less than 10^{-4} Pa.

https://doi.org/10.1017/S0022377809990717 Published online by Cambridge University Press

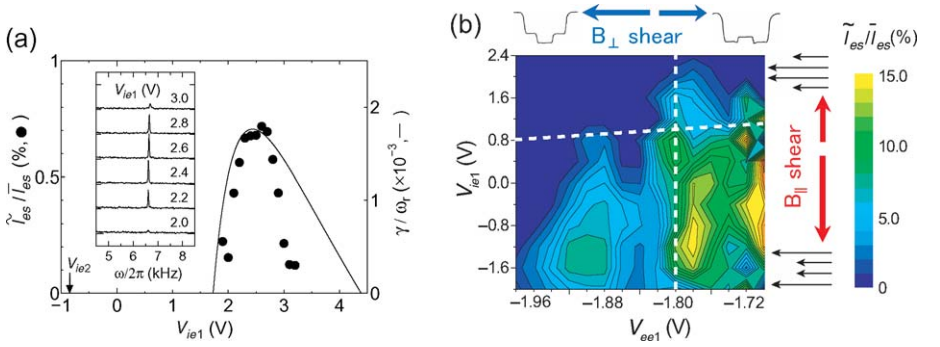


Figure 2. (Color online) (a) Frequency spectra of electron saturation current I_{es} and normalized fluctuation amplitudes as a function of V_{ie1} for $V_{ie2} = -0.8$ V in the parallel shear case. Theoretical growth rate of the drift-wave instability is also plotted (solid line). (b) Contour view of normalized fluctuation amplitudes as functions of V_{ie1} and V_{ee1}.

2.2. Experimental results and discussion

In the case where the parallel flow shear is generated, a drift-wave instability is found to be excited where $V_{ee1,2,3}$ are fixed to generate no perpendicular shear. Figure 2(a) presents frequency spectra of electron saturation current I_{es} of a probe and normalized fluctuation amplitudes $\tilde{I}_{es}/\bar{I}_{es}$ of the electron saturation current as a function of V_{ie1} for $V_{ie2} = -0.8$ V, $V_{ie3} = 0$ V at $r = -1.0$ cm. Here the position of $r = -1.0$ cm corresponds to the central shear region between the first and second ion emitters. When V_{ie1} is almost the same as V_{ie2}, the fluctuation is not excited. Once V_{ie1} exceeds a certain threshold, the fluctuation with the frequency of about 6.5 kHz is observed to grow as V_{ie1} becomes large. When V_{ie1} is increased more, $\tilde{I}_{es}/\bar{I}_{es}$ attains a maximum value and gradually decreases after that. In order to identify the parallel-shear enhanced drift-wave instability, the theoretical growth rate γ as a function of V_{ie1} is calculated using the kinetic dispersion relation and is plotted in Fig. 2(a) (solid line). The experimental results are in good agreement with the theoretical curves and it turns out that the growth rate changes into positive when V_{ie1} exceeds the threshold and gradually increases with an increase in V_{ie1}. This means that the ion-frame phase velocity of the fluctuation becomes large due to the presence of the parallel shear, and, thus, the effect of the ion Landau damping on the waves is reduced. For larger V_{ie1}, however, the growth rate saturates and gradually decreases with a further increase in V_{ie1}. When the phase velocity exceeds the ion flow velocity, *i.e.* the relative electron-ion drift velocity in the ion frame, due to the increase in V_{ie1}, the effect of the inverse electron Landau damping in the ion frame is reduced, which leads to the stabilization of the waves [3, 4].

Then, we obtain the contour view of the normalized fluctuation amplitude as functions of the parallel (V_{ie1}) and perpendicular (V_{ee1}) flow shears as shown in Fig. 2(b), where the bias voltages of the other emitters are fixed. Black arrows described at right axis mean the parallel ion flow velocity and solid curves described at superior axis mean the radial potential profiles, which are controlled by V_{ie1} and V_{ee1}, respectively, corresponding to the variation of the parallel and perpendicular flow velocity shears. Here, horizontal and vertical dotted lines in Fig. 2(b) denote the situations in the absence of the parallel and perpendicular shears, respectively. When the perpendicular shear is superimposed on the parallel shear, the drift wave

https://doi.org/10.1017/S0022377809990717 Published online by Cambridge University Press

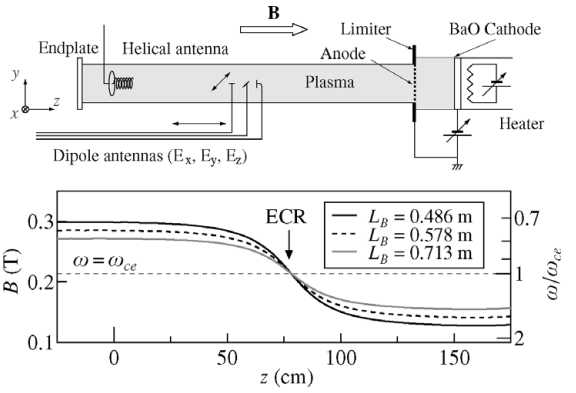


Figure 3. Schematic of experimental setup and external magnetic field configuration. The microwave frequency is $\omega/2\pi = 6$ GHz.

excited by the parallel shear is found to be suppressed by the perpendicular shear independent of the sign of the perpendicular shear. Furthermore, we can observe two characteristic fluctuation peaks depending on the perpendicular shear strength, which are defined as fluctuations A ($V_{ee1} \sim -1.90$ V, $V_{ie1} \sim -1.5$ V) and B ($V_{ee1} \sim -1.78$ V, $V_{ie1} \sim -1.1$ V). To readily identify the azimuthal component of each fluctuation's wave vector, we measure two-dimensional (x, y) profiles of fluctuation phase in the plasma-column cross section [4]. In the case of the small perpendicular shear strength, *i.e.* fluctuation B, the azimuthal mode is found to be $m = 3$. On the other hand, in the presence of the relatively large perpendicular shear, *i.e.* fluctuation A, the azimuthal mode changes into $m = 2$. With an increase in the parallel shear strength, it is clarified that $m = 3$ mode ($V_{ee1} \sim -1.78$ V) is first excited and $m = 2$ mode ($V_{ee1} \sim -1.90$ V) needs strong parallel shear strength to be excited. Based on these results, the strength of the perpendicular shear is found to be important in modifying the parallel shear-enhanced instability [14].

3. Damping of electromagnetic waves due to polarization reversal

Electromagnetic waves with ECR frequency have been significant research subjects for basic physical problems, electron heating, plasma production and so on. A LHPW, which has been believed not to be related to ECR, is experimentally demonstrated to be anomalously absorbed near the ECR point. In order to clarify its mechanism, propagation and absorption of the electromagnetic wave with the ECR frequency are investigated.

3.1. Experimental setup

Experiments are performed in the Q_T—Upgrade machine of Tohoku University as shown in Fig. 3, which has a cylindrical vacuum chamber about 450 cm in length and 20.8 cm in diameter. A coaxial bounded plasma is produced by a direct current discharge between an oxide cathode and a tungsten mesh anode with a limiter in low-pressure argon gas (90 mPa). The formation of a clear boundary between the plasma and the vacuum region is realized by using the limiter, which also can control the plasma radius r_p in the range of 2.5–4 cm. The plasma column is terminated on a glass endplate located at the opposite end of the plasma source.

https://doi.org/10.1017/S0022377809990717 Published online by Cambridge University Press

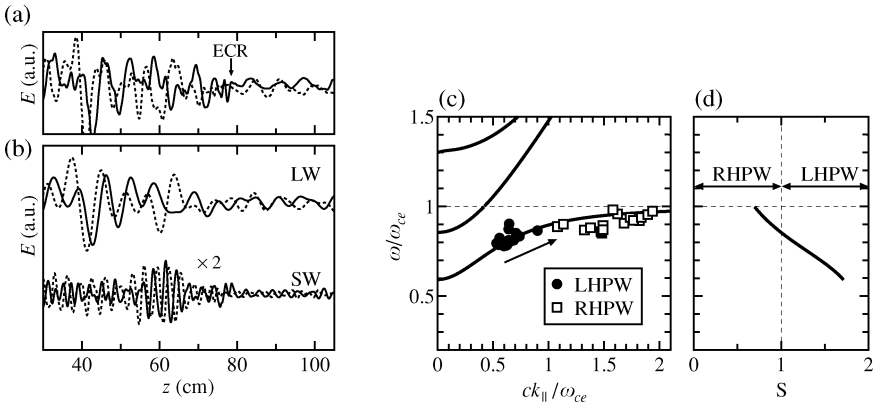


Figure 4. (a) Interferometric wave patterns of E_x and E_y in launching the LHPW. (b) LW and SW components included in the wave pattern of Fig. 4(a). (c) Calculated dispersion relations (solid lines) together with the experimental dispersions obtained from the LHPW (closed circle) and the RHPW (open square). (d) Calculated polarization index S corresponding to the dispersion curve, which agrees with the experimental dispersion.

Under these conditions, the electron density and temperature are $n_e \sim 9{\times}10^{10}$ cm^{-3} and $T_e \sim 3$ eV, respectively. Magnetic field configurations are inhomogeneous as presented in Fig. 3, where a characteristics length L_B of magnetic field gradient is defined as $L_B = [(1/B)dB/dz]^{-1}$ and the condition of $\omega_{pe} < \omega_{ce}$ is satisfied in the plasma column ($\omega_{pe}/2\pi$: electron plasma frequency, $\omega_{ce}/2\pi$: electron cyclotron frequency). A microwave (frequency $\omega/2\pi = 6$ GHz, power 150 mW) is selectively launched in the high magnetic field region as the LHPW by a helical antenna ($z = 0$ cm) [6]. The wave propagates toward the ECR point ($z = 78$ cm) satisfying the condition of $\omega/\omega_{ce} < 1$. The wave patterns are obtained with an interference method through axially and radially movable balanced dipole antennas, which can receive each component of electric fields of the wave, *i.e.* E_x, E_y, and E_z.

3.2. Experimental results and discussion

Figure 4(a) shows typical interferometric wave patterns of E_x (solid line) and E_y (dotted line) at the radial center of the plasma column, where a solid arrow indicates the ECR point of the launched wave. The wave patterns denote the unexpected damping of the wave near the ECR point in spite of the selective launch of the LHPW. The long (LW) and short (SW) wavelength components decomposed from the observed wave patterns in Fig. 4(a) are presented in Fig. 4(b), which can be obtained by performing the Fourier analysis. It is to be noted that the LW damps and SW grows around $z = 60$ cm in Fig. 4(b). Moreover, it is obviously observed that the phase differences between E_x and E_y for the LW and the SW are oppositely shifted. The phase differences and the direction of magnetic-field lines let us identify that the polarizations of the LW and the SW are left-handed and right-handed, respectively. Therefore, Fig. 4(b) indicates that the LHPW damps and the right-hand polarized wave (RHPW) grows around $z = 60$ cm, *i.e.* the polarization reversal from the LHPW to the RHPW and the resultant absorption of the launched LHPW are demonstrated. We mention that the radial profile of E_z experimentally gives $m = 0$, where m is an azimuthal mode number.

https://doi.org/10.1017/S0022377809990717 Published online by Cambridge University Press

In order to clarify the mechanism of the polarization reversal, the theoretical dispersion relation and wave polarizations for $m = 0$ mode are compared with the experimental results. A dispersion relation including the effect of the radial boundary and a polarization index S [$\equiv (|E_x + iE_y|)/(|E_x - iE_y|)$] are given in [15, 16], where $0 < S < 1$ and $1 < S < \infty$ represent right-handed and left-handed polarizations, respectively. The calculated dispersion relations are presented in Fig. 4(c) as solid lines together with the experimental dispersion relations obtained from the LHPW (closed circle) and the RHPW (open square) components, namely, the LW in the high magnetic field region and the SW growing near the ECR point in Fig. 4(b). One of the calculated curves is in good agreement with the experimental ones. The polarization index S corresponding to the dispersion curve, which agrees with the experimental values, is drawn in Fig. 4(d) in order to theoretically verify the polarization reversal. The value of S is larger than unity in the range of $\omega/\omega_{ce} < 0.85$, *i.e.* the polarization is left-handed. As the wave approaches the ECR point ($\omega/\omega_{ce} = 1$), the value of S becomes smaller than unity. That is to say, the polarization reversal from the LHPW to the RHPW is also theoretically demonstrated. As a result, the launched LHPW is absorbed by ECR, because the wave polarization becomes right-handed in obedience to the dispersion relation in the bounded plasma.

4. Pair-ion plasmas

Wave propagations not only in the above-mentioned ordinary electron-ion plasmas but also in pair plasmas consisting of only positive- and negative-charged particles with an equal mass have been investigated experimentally and theoretically from the viewpoint of finding new features of the wave in such novel plasmas. Spatial–temporal parity is kept in pair plasmas and this is quite different from the ordinary electron-ion plasmas. We have developed a novel method for generating a pair-ion plasma that consists of only positive and negative ions of equal mass using fullerene [17–20].

4.1. Experimental setup

A pair-ion plasma source with fullerene ion species consists of an electron-beam gun, an ion production cylinder and a magnetic filter. The electron-beam gun is set inside the ion production cylinder (8-cm diameter and 30-cm length) with a thin annulus (inner diameter 3-cm and 0.1-cm thickness) made of copper. The plasma source is installed in a grounded vacuum chamber of 15.7-cm diameter and 260-cm length, as shown schematically in Fig. 5. A uniform magnetic field of $B = 0.2$ T is applied using solenoid coils and the background gas pressure is 2×10^{-4} Pa. A tungsten wire cathode with a ring structure of 5-cm diameter is resistively heated to over 2000°C. The wire cathode is biased at voltage V_k (< 0 V) with respect to a grounded grid anode set at less than 0.5 cm in front of the cathode. A stainless steel disk of 4-cm diameter is concentrically welded onto the grid anode. Thermally emitted low-energy electrons (~ 0.2 eV) are accelerated by the electric field between the cathode and the anode, and form a hollow electron beam. The cylinder and the annulus are grounded, and the beam flows along the magnetic (B) field lines and is terminated at the annulus. The beam energy E_e can be controlled in the range of 0—150 eV by changing V_k. The electron beam with an annular cross section collides with neutral C_{60}, and C_{60}^+ is produced by impact ionization. Then low-energy electrons

https://doi.org/10.1017/S0022377809990717 Published online by Cambridge University Press

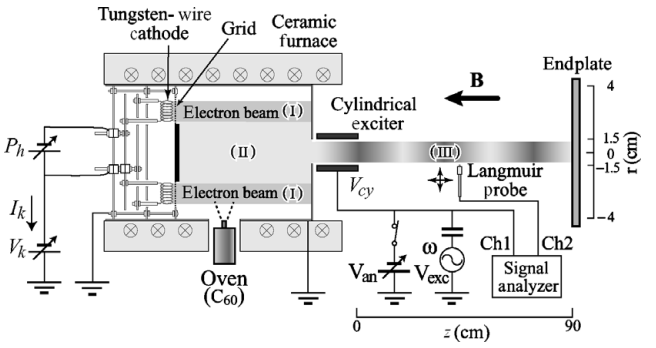


Figure 5. Schematic drawing of experimental setup. Longitudinal electrostatic wave modes propagating along B-field lines are excited by a cylindrical exciter. Region (I) is the hollow electron-beam part, region (II) is the magnetically filtered part and region (III) is the experimental part.

are simultaneously produced and they contribute to producing negative ions, C_{60}^- ions, due to electron attachment. To produce C_{60}^+ and C_{60}^- concurrently, it is essential that C_{60} has the feature of electron attachment over a broad-energy range. The chamber wall is grounded and an endplate is maintained at a floating potential. For analytic convenience, the whole space of the plasma is divided into three regions, (I), (II) and (III). The hollow electron-beam region is the fullerene-ion production region and is called region (I). Only C_{60}^+ and C_{60}^- are expected to inwardly diffuse across the B-field lines and exist in the center of the cylinder, region (II), and the electron-free pair-ion plasma generation occurs here. C_{60}^+ and C_{60}^- flow along the B-field lines and pass through the annular hole toward an experimental region, region (III). A cylindrical electrode is set in front of the annular hole between regions (II) and (III). The electrode can be biased at V_{an} superimposed by V_{exc} ($V_{cy} = V_{an} + V_{exc}$), where V_{an} is a DC voltage and V_{exc} is an AC voltage of frequency $\omega/2\pi$. The exit position of the electrode is defined as $z = 0$ cm, and the pair-ion plasma is terminated at the endplate ($z = 90$ cm). Plasma parameters in region (III) are measured using Langmuir probes.

4.2. Experimental results and discussion

When the electron-beam energy E_e increases from 0 eV, the pair-ion plasma begins to be generated. The plasma density gradually increases and almost saturates at around $E_e = 150$ eV. The number of C_{60}^- produced is thought to be smaller than that of C_{60}^+ produced in region (I), because a part of low-energy electrons produced in the process of C_{60}^+ production contributes to produce C_{60}^-. But the densities of C_{60}^+ and C_{60}^- are almost the same for the reason of ambipolar diffusion in the magnetic filter between regions (I) and (II). The current voltage (I_p—V_p) characteristic of the probe is almost symmetrical. The plasma potential is close to 0 V, which is almost equal to the potential of the grid and the annulus. The static potential structures including sheaths are not to be formed in the pair-ion plasma because the mobilities of the ions are almost same. The plasma density and the ion temperatures are calculated from the probe characteristics. The density is 1–2 × 10^8 cm^{-3} at $E_e = 100$ eV, while the temperatures of C_{60}^+ and C_{60}^-, T_+ and T_-, are 0.3–0.5 eV.

The cylindrical electrode set in front of the annular hole between regions (II) and (III) is biased at V_{cy}. The plasma density can be modulated by temporally changing

https://doi.org/10.1017/S0022377809990717 Published online by Cambridge University Press

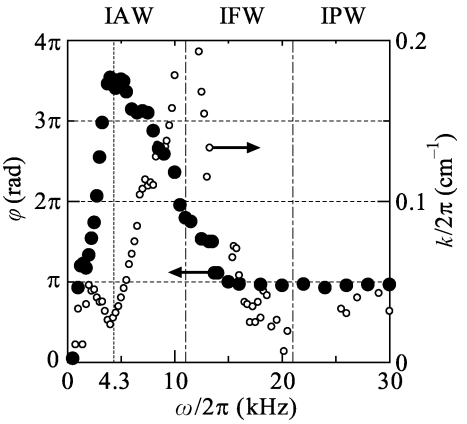


Figure 6. Phase lag φ between $\tilde{I}_+$ and $\tilde{I}_-$ is defined as $\tilde{I}_+ = \tilde{I}_-\exp(i\varphi)$. The phase-lag spectrum and the dispersion relation are shown by closed circles and open circles, respectively.

V_{cy} ($V_{exc} \neq 0$), and longitudinal electrostatic modes can be excited in region (III). In the present situation it is extremely difficult to excite electromagnetic modes relevant to the plasma because the density and the temperature are relatively low and the induction current of the ions is very small. Hence, longitudinal electrostatic modes are excited in region (III) by the cylindrical exciter. The properties of mode propagation along the B-field lines are measured at $r = 0$ cm, $z = 4$—6 cm and $E_e = 100$ eV. The phase delay between the excited and the fluctuation signals is measured at each $z = 4$, 5 and 6 cm, and the wave number k (wave length) of the propagating modes is obtained from the averaged phase delay. The frequency $\omega/2\pi$ of the excited signal is changed from 0.1 to 50 kHz. Temporal variations of the positive- and negative-ion densities are measured as $\tilde{I}_+$ and $\tilde{I}_-$, which indicate the oscillating components of the positive- and negative-saturation currents of the probe, corresponding to those of the positive- and negative-ion densities ($\tilde{n}_+$ and $\tilde{n}_-$), measured at $r = 0$ cm and $z = 5$ cm, respectively. Here, a phase lag φ between the oscillating components $\tilde{I}_+$ and $\tilde{I}_-$ is defined as $\tilde{I}_+ = \tilde{I}_-\exp(i\varphi)$, which becomes synonymous with $\tilde{n}_+ = \tilde{n}_-\exp(i\varphi)$. As a detailed expression of the frequency dependence of φ, a phase-lag spectrum and the dispersion relation of the propagating modes are shown in Fig. 6, where closed and open circles denote the phase-lag spectrum and the dispersion relation, respectively. There are three modes in the measured dispersion relations, $\omega/2\pi < 12$ kHz, $12 < \omega/2\pi < 20$ kHz and $\omega/2\pi > 20$ kHz, which we refer to as an ion acoustic wave (IAW), an intermediate-frequency wave (IFW) and an ion plasma wave (IPW), respectively. IFW has the feature that the group velocity is negative but the phase velocity is positive, *i.e.* the mode resembles a backward wave. It is definitely shown that IAW divides into two branches at around the ion cyclotron frequency $\omega_c/2\pi = 4.3$ kHz. The mode in $2.5 < \omega/2\pi < 4.3$ kHz is a backward-like mode and apparently analogous to IFW joining IAW and IPW. φ drastically changes for variations in $\omega/2\pi$ below 15 kHz. The phase lag largely increases in proportion to $\omega/2\pi$ in the low-frequency range of IAW ($\omega/2\pi < \omega_c/2\pi$). The phase lag becomes $\varphi = 7\pi/2$ at $\omega_c/2\pi$ and the phase lag inversely decreases in proportion to $\omega/2\pi$ in $\omega_c/2\pi < \omega/2\pi < 15$ kHz. The phase lags of IFW and IPW in $\omega/2\pi > 15$ kHz are π independent of $\omega/2\pi$. The

https://doi.org/10.1017/S0022377809990717 Published online by Cambridge University Press

φ property of IAW in the pair-ion plasma is unique, because the phase lag between the electron and ion densities in ordinary electron-ion plasmas usually has little change. The backward-like mode joining the two branches of IAW is apparently analogous to IFW in the dispersion relation, but the φ property is quite different, that is, the backward-like mode has a strong frequency dependence of φ, but IFW does not. The phase lags of IFW and IPW are reversed, which means that a charge separation is realized and electrostatic-potential structures are formed in the pair-ion plasma in the dynamical state. This is in contrast to the measured result that the electrostatic-potential structures including sheaths are almost not formed in the stationary state. In ordinary electron-ion plasmas, φ is close to zero for IAW and φ cannot be defined for the electron plasma wave (synonymous with IPW in the pair-ion plasma) because the ion response is very slow compared to the electron response and the ion-density fluctuation is ignored. Thus, IFW and IPW with $\varphi \approx \pi$ reflects a special situation.

4.3. Evolution of pair-ion plasmas

The response frequency of the pair-ion plasma is limited to narrow bandwidths below 50 kHz because of the massive ions. In order to investigate more extensive physical properties of pair plasmas, particularly wave-propagation characteristics at higher frequencies, the development of a hydrogen pair-ion plasma source has been started [21], because hydrogen atomic pair ions, H^+ and H^- ions, are the lightest ions with high- response frequencies to electromagnetic fields. Several difficulties exist in this development that should be overcome. The most crucial problem is the efficient production of hydrogen negative ions, H^- ions. The research and the development of the negative ion sources have been extensively performed for more than 20 years in connection with neutral beam injection (NBI) heating for fusion-oriented plasmas and ion guns for the run-up of proton accelerators. The production method of H^- ions is classified into a volume production and a surface production due to contact ionization. The electronic work function on the surface of extraction electrodes becomes lower due to thin cesium coating. Surface electrons of the electrodes easily transfer to hydrogen atoms approaching the surface, and the production efficiency of H^- ions improves. Cesium with a low evaporation temperature, however, is easily vaporized and ionized, the ions come to be mixed in the plasma, thus, cesium cannot be used here for the generation of the hydrogen pair-ion plasma. The generation of the pair-ion plasma requires an equal production of H^+ and H^- ions in quantity and no existence of impurities such as electrons and the other ions. It is difficult to satisfy these conditions if the contact ionization or the volume production is adopted. The production process of the atomic ions is considered so that atomic hydrogen is produced in the first stage and ionized in the second stage. Now, it is tried to attain the generation of hydrogen pair-ion plasma in such a way that a hydrogen discharge plasma is irradiated to a transition-metal porous catalyst and the hydrogen pair ions are produced from the backside of the irradiation plane.

5. Conclusions

We have performed the basic-plasma experiments on the flow shears, the polarization reversal and the pairions, and obtained new aspects on the plasma wave and instability phenomena.

https://doi.org/10.1017/S0022377809990717 Published online by Cambridge University Press

First, parallel and perpendicular plasma flow velocity shears are independently controlled and superimposed in magnetized plasmas using a novel plasma-synthesis method with concentrically three-segmented electron and ion emitters. The parallel shear is observed to destabilize the drift-wave instability depending on the shear strength, while the perpendicular shear superimposed on the parallel shear is demonstrated to suppress the instability even in the presence of the parallel shear.

Secondly, the left-hand polarized wave is demonstrated to be absorbed near the electron-cyclotron resonance point in an inhomogeneously magnetized plasma as a result of the polarization reversal to the right-hand polarized wave, which is quantitatively explained in terms of the dispersion relation including the effect of the radial boundary condition.

Thirdly, excited electrostatic modes are investigated in the pair fullerene-ion plasma. Ion acoustic wave, new intermediate frequency wave and ion plasma wave with plane wave structures exist in the plasma, and another new backward wave in IAW frequency range is clearly detected. Furthermore, we are going to generate a pair-ion plasma using ions with light mass and to investigate the properties of linear waves and nonlinear waves such as pulses, shock waves and holes.

Acknowledgements

We express our gratitude to Professor P. K. Shukla, Professor M. Koepke, Dr. G. Ganguli, Dr. R. Ichiki and Dr. K. Takahashi for their collaboration. This work was supported by a Grant-in-Aid for Scientific Research from the Ministry of Education, Culture, Sports, Science and Technology, Japan.

References

[1] Agrimson, E., D'Angelo, N. and Merlino, R. L. 2001 Excitation of ion-acoustic-like waves by subcritical currents in a plasma having equal electron and ion temperatures. *Phys. Rev. Lett.* **86**, 5282–5285.

[2] Teodorescu, C., Reynolds, E. W. and Koepke, M. E. 2002 Observation of inverse ion-cyclotron damping induced by parallel-velocity shear. *Phys. Rev. Lett.* **89**, 1050011–4.

[3] Kaneko, T., Tsunoyama, H. and Hatakeyama, R. 2003 Drift-wave instability excited by field-aligned ion flow velocity shear in the absence of electron current. *Phys. Rev. Lett.* **90**, 125001:1–4.

[4] Kaneko, T., Reynolds, E. W., Hatakeyama, R. and Koepke, M. E. 2005 Velocity-shear-driven drift waves with simultaneous azimuthal modes in a barium-ion Q-machine plasma. *Phys. Plasmas* **12**, 102106:1–6.

[5] Hatakeyama, R. and Kaneko, T. 2004 Sheared flow excitation and suppression of electrostatic instabilities in laboratory collisionless magnetoplasmas. *Phys. Scripta* **T107**, 200–203.

[6] Kaneko, T., Murai, H., Hatakeyama, R. and Sato, N. 2001 Experimental evidence for spatial damping of left-hand circularly polarized waves in an electron cyclotron resonance region. *Phys. Plasmas* **8**, 1455–1458.

[7] Iwamoto, N. 1993 Collective modes in nonrelativistic electron-positron plasmas. *Phys. Rev.* E **47**, 604–611.

[8] Stewart, G. A. 1993 Nonlinear electrostatic waves in equal-mass plasmas. *J. Plasma Phys.* **50**, 521–539.

[9] Zank, G. P. and Greaves, R. G. 1995 Linear and nonlinear modes in nonrelativistic electron-positiron plasmas. *Phys. Rev.* E **51**, 6079–6090.

[10] Surko, C. M., Leventhal, M. and Passner, A. 1989 Positron plasma in the laboratory. *Phys. Rev. Lett.* **62**, 901–904.

https://doi.org/10.1017/S0022377809990717 Published online by Cambridge University Press

[11] Boehmer, H., Adams, M. and Rynn, N. 1995 Positron trapping in a magnetic mirror configuration. *Phys. Plasmas* **2**, 4369–4371.

[12] Greaves, R. G. and Surko, C. M. 2001 Radial compression and inward transport of positron plasmas using a rotating electric field. *Phys. Plasmas* **8**, 1879–1885.

[13] Kaneko, T., Odaka, Y., Tada, E. and Hatakeyama, R. 2002 Generation and control of field-aligned flow velocity shear in a fully ionized collisionless plasma. *Rev. Sci. Instrum.* **73**, 4218–4222.

[14] Kaneko, T., Tamura, S., Ito, A. and Hatakeyama, R. 2008 Drift-wave instabilities modified by parallel and perpendicular flow velocity shears in magnetized plasmas. *Plasma Fusion Res.* **3**, S1011:1–5.

[15] Takahashi, K., Kaneko, T. and Hatakeyama, R. 2005 Polarization-reversal-induced damping of left-hand polarized wave on electron-cyclotron resonance. *Phys. Rev. Lett.* **94**, 215001:1–4.

[16] Takahashi, K., Kaneko, T. and Hatakeyama, R. 2005 Effects of polarization reversal on localized-absorption characteristics of electron cyclotron wave in bounded plasmas. *Phys. Plasmas* **12**, 102107:1–7.

[17] Oohara, W. and Hatakeyama, R. 2003 Pair-ion plasma generation using fullerenes. *Phys. Rev. Lett.* **91**, 205005:1–4.

[18] Oohara, W. and Hatakeyama, R. 2005 Electrostatic waves in a paired fullerene-ion plasma. *Phys. Rev. Lett.* **95**, 175003:1–4.

[19] Oohara, W. and Hatakeyama, R. 2007 Basic studies of the generation and collective motion of pair-ion plasmas. *Phys. Plasmas* **14**, 055704:1–7.

[20] Oohara, W., Kuwabara, Y. and Hatakeyama, R. 2007 Collective mode properties in a paired fullerene-ion plasma. *Phys. Rev.* E **75**, 056403:1–9.

[21] Oohara, W. and Fukumasa, O. 2009 Catalytic effect on ionization of hydrogen. *J. Plasma Fusion Res. series* **8**, 860–864.

https://doi.org/10.1017/S0022377809990717 Published online by Cambridge University Press